THE ASTROPHYSICAL JOURNAL, 214:584–597, 1977 June 1

STABLEST SHAPES FOR AN AXISYMMETRIC BODY OF GRAVITATING, INCOMPRESSIBLE FLUID*

PHILIP S. MARCUS
Joseph Henry Laboratories, Princeton University
WILLIAM H. PRESS†
Center for Astrophysics, Harvard College Observatory, and Department of Physics, Harvard University
AND
SAUL A. TEUKOLSKY†
Physics Department and Center for Radiophysics and Space Research, Cornell University
Received 1976 September 10; revised 1976 November 22

ABSTRACT

A numerical method for computing the total energy of self-gravitating, incompressible, rotating, axisymmetric fluid bodies is presented. Then, using a minimization technique, the stablest axisymmetric shapes are found for fluids having the same angular momentum distribution as the Maclaurin spheroids. For small angular momenta the Maclaurin spheroid is a minimum-energy configuration; above a certain value a new, toroidal family of differentially rotating figures becomes the stable minimum-energy shape. Just below this critical value the spheroids are stable to small perturbations, but the corresponding toroids have lower energy. The family of "Mestel disks" (mass $\propto 1/r$, flat rotation curve) with this same angular momentum distribution are equilibria, but they are always unstable. Similar conclusions hold for other angular momentum distributions also investigated. These results may clarify the "ring formation" stage of some realistic collapse models, and may also support the hypothesis of massive galactic halos.

Subject headings: galaxies: formation — hydrodynamics — instabilities — rotation

I. INTRODUCTION

We have investigated some equilibrium and nonequilibrium configurations of an axisymmetric mass of gravitating, incompressible fluid, which is rapidly and differentially rotating. Some curious results have emerged, as have some efficient numerical techniques which may be extendible to more realistic problems in the structure of rotating stars and galaxies.

Since our model system is so highly idealized, we will state the case for its astrophysical relevance at this point, rather than later. The underlying problem is the collapse of a rapidly rotating gas mass to form a star or stellar association; or of a rapidly rotating mass of gas and/or stars to form a galaxy. In the physics of both collapse problems, one would like to distinguish the dynamical features which originate with just Newton's laws of motion and gravitation, from features which depend on much messier and more complicated "transport" phenomena—radiation losses, angular momentum transport by turbulence or hydromagnetic instability, convection, violent stellar relaxation, and so on. Of course, these transport effects are the crux of any realistic calculations (such as those of Larson 1972 for galaxies, or Black and Bodenheimer 1976 for stars). But transport effects are difficult to model accurately, so it is not always possible to know which aspects of a "realistic" calculation are in fact realistic, and which are artifacts of the model's assumptions. A good intuitive appreciation of the purely dynamical properties of rotating, gravitating systems should help mitigate this problem. Even the purely dynamical phenomena are sufficiently varied, however, that this appreciation must be developed through a variety of model investigations of idealized systems.

The approach of this paper is to explore, numerically, the total energy (gravitational plus rotational) of an axisymmetric fluid mass, as a function of its physical shape, and to apply a highly efficient minimization algorithm to find local minima in this energy (which correspond to equilibrium configurations). We are not restricted to small changes in shape; we will smash equilibrium spheroids into pancakes or tori, and see whether they return to their old minima, or to new ones. The rule of the game is that each mass element (a ring, because of axisymmetry) has its angular momentum specified initially and conserved thereafter; there is no viscous transport of angular momentum. (See Gott and Thuan 1976 for discussion of the situations in galaxy formation where this assumption might be realistic.)

* Supported in part by the National Science Foundation, grants GP-30799X, PHY76-14852, and PHY76-07297.
† Alfred P. Sloan Foundation Research Fellow.

The sequence of physical shapes taken by a galaxy or star in its collapse will not, in general, be exactly a "valley" of the energy surface that we are exploring; but it may well be "close" to a valley, especially if dissipation time scales are comparable to or larger than dynamical time scales. A dynamic evolution must in any case terminate at a local minimum of the energy surface. So, given an initial configuration, we may want to think of its steepest downhill valley as a "preferred" channel for evolution. Often this channel will be competing with other channels that we are not modeling, such as an efficient mechanism for angular momentum transport. In other cases there may be unmodeled channels which can act cooperatively with modeled ones. For example, many of our configurations are likely to be unstable not only against nonaxisymmetric instabilities (not modeled) but also against substantial radial readjustment (which we see in the energy surface). One has a feeling that these changes are roughly "orthogonal," at least initially, so both channels probably act cooperatively, at least for a while, with the fluid both fragmenting and radially readjusting itself.

Here are some more specific questions that we will address in this study: (1) What is the shape of the *stable* continuation of the Maclaurin sequence (uniformly rotating, flattened spheroids) at angular momenta above the onset of axisymmetric instabilities? (2) Are the configurations of Mestel (1963), which have galaxy-like rotation curves, radially stable? If not, what stable configuration do they go to? (3) Given an angular momentum distribution, can there be more than one *stable* equilibrium configuration? If there is more than one, then the shape of a galaxy or star might depend on how it "happened" to collapse; and under a sufficiently large perturbation it might dynamically switch to a new shape. (In fact, we do find this effect in our axisymmetric inviscid models.)

Section II of this paper concerns itself with a problem in "classical" potential theory: computing the gravitational energy of a fluid mass as a finite superposition of cylindrical shells and estimating the truncation error inherent in this method. The utility of this method is that it reduces the subsequent calculation of gravitational potentials to one-dimensional (from two). For flat systems, we think that this technique is superior to that of using concentric spheroidal shells, as in Cameron and Pine (1973).

In § III we prove that our minimization procedure is equivalent to standard structure equations, and we review the Fletcher-Powell (1963) minimization algorithm, which we have found to be very efficient. Masses with the angular-momentum distribution of a Maclaurin spheroid (or rigidly rotating sphere) are studied in § IV. Some other angular-momentum distributions are investigated in § V. Finally, § VI summarizes our findings.

II. GRAVITATIONAL POTENTIAL ENERGY OF AN AXISYMMETRIC, INCOMPRESSIBLE FLUID

a) Discretized Calculation

Suppose that a fluid mass of density ρ has an axis of rotational symmetry perpendicular to the axis. In cylindrical coordinates (R, ϕ, z), suppose that the fluid surface is at $z = \pm h(R)$, where $h(R)$ is a single-valued function. (Reflection symmetry and single-valuedness are not absolutely essential for what follows, but they make the calculation simpler.)

Next, discretize the calculation by dividing the body into N radial zones, where the boundaries of the zones are the cylinders $R = R_i$, $i = 0, 1, \ldots, N$, where $R_0 \equiv 0$, and R_N is the farthest radial extent of the fluid. The gravitational potential energy of the fluid is now a sum of interaction energies between different zones, $W_{ij}^{\rm int}$ $(1 \leq i < j \leq N)$ and self-energies of the zones, $W_i^{\rm self}$ $(1 \leq i \leq N)$. We will approximate the $W_{ij}^{\rm int}$ by calculating exactly the interaction energy between two *infinitesimally thin* cylindrical shells with radii a_i and a_j, masses M_i and M_j, and semiheights h_i and h_j, given by

$$a_i \equiv \tfrac{1}{2}(R_{i-1} + R_i)\,, \tag{2.1}$$

$$h_i \equiv (R_i^2 - R_{i-1}^2)^{-1} \int_{R_{i-1}}^{R_i} 2h(R)RdR = \frac{M_i}{2\pi\rho(R_i^2 - R_{i-1}^2)} \tag{2.2}$$

(and likewise for j). We approximate the self-energy, $W_i^{\rm self}$, by calculating one-half the interaction energy of two shells like the above, each of mass M_i and semiheight h_i, and located at fractional distances 0.3844 and 0.6116 into the ith zone. These approximations may sound arbitrary; but we show in § II*b* that they result in a value for the potential energy which is exact to order $1/N$, and has fractional errors only at order $1/N^2$; in other words, 30 zones will give accuracy to the 0.1% level.

Now to calculate the interaction energy between infinitesimally thin shells, we write

$$\begin{aligned} W_{ij}^{\rm int} &= -\frac{M_iM_j}{8\pi h_ih_j}\int_0^{2\pi} d\phi \int_{-h_i}^{h_i} dz \int_{-h_j}^{h_j} dz'[(z - z')^2 + a_i^2 + a_j^2 - 2a_ia_j\cos\phi]^{-1/2} \\ &= \frac{-M_iM_j}{h_ih_j}\int_0^{\infty} dk J_0(ka_j)J_0(ka_i)\left[\frac{h_>}{k} - \frac{1}{k^2}\exp(-kh_>)\sinh(kh_<)\right]. \end{aligned} \tag{2.3}$$

Here we have chosen units with the gravitational constant G equal to unity and used the standard techniques of,

e.g., Morse and Feshbach (1953, § 10.3); $h_>(<)$ is the greater (lesser) of h_i and h_j. If we define a function $G(\alpha, \beta)$ by

$$G(\alpha, \beta) \equiv \int_0^\infty dk \left[\frac{\beta}{k} - \frac{1}{k^2} \exp(-\beta k)\right] J_0(k\alpha) J_0(k) , \tag{2.4}$$

then equation (2.3) becomes

$$W_{ij}^{\text{int}} = \frac{-M_i M_j a_j}{2h_i h_j} \left[G\left(\frac{a_i}{a_j}, \frac{h_i + h_j}{a_j}\right) - G\left(\frac{a_i}{a_j}, \frac{|h_i - h_j|}{a_j}\right)\right] . \tag{2.5}$$

We discuss the relation of $G(\alpha, \beta)$ to known functions, and give efficient numerical methods for calculating it, in § II*c*.

One might ask, Why introduce a function G that has to be tabulated numerically? Why not directly define a tabulated function that is the interaction energy of the ith and jth shells (when multiplied by $M_i M_j$, say)? The answer is that this function would be a function of three variables instead of two: from the four lengths a_i, a_j, h_i, and h_j, one can form three independent dimensionless ratios. Thus, it is in fact somewhat surprising that we can calculate W_{ij}^{int} from a function G of two dimensionless variables only. The reason for this is that there is an underlying, hidden symmetry in the problem: using superposition arguments, the two h's can be subsumed into a single vertical displacement between two semi-infinite cylinders.[1] The geometrical details will not concern us here.

For the self-energy of a single zone we have, in the approximation described above,

$$W_i^{\text{self}} = -\frac{M_i^2}{4h_i^2} (0.6116R_i + 0.3884R_{i-1}) G\left(\frac{0.3884R_i + 0.6116R_{i-1}}{0.6116R_i + 0.3884R_{i-1}}, \frac{2h_i}{0.6116R_i + 0.3884R_{i-1}}\right) , \tag{2.6}$$

where we have used $G(\alpha, 0) = 0$ (see § II*c* below). The total gravitational potential energy W now follows from equations (2.5) (2.6), and

$$W = \sum_{1 \le i < j \le N} W_{ij}^{\text{int}} + \sum_{1 \le i \le N} W_i^{\text{self}} . \tag{2.7}$$

In subsequent sections we will want to know not only W, but also the generalized gravitational forces associated with changes in the radii R_i, namely,

$$F_i^W \equiv -\frac{\partial W}{\partial R_i} . \tag{2.8}$$

These are readily calculated from equations (2.1), (2.2), (2.8), and (2.4)–(2.7) in terms of two new functions:

$$g(\alpha, \beta) \equiv \frac{\partial G(\alpha, \beta)}{\partial \beta} ,$$

$$\mathcal{G}(\alpha, \beta) \equiv \frac{\partial G(\alpha, \beta)}{\partial \alpha} . \tag{2.9}$$

These functions will also be considered below in more detail.

b) Error Estimates

The reader who is satisfied that equation (2.7) has truncation errors only of order $1/N^2$ can omit this section. Consider an approximation intermediate between our W_{ij}^{int} and the exact $W_{ij}^{\text{int}(E)}$: let $W_{ij}^{\text{int}(I)}$ be the interaction energy of two cylindrical shells of finite thickness, extending from R_{i-1} to R_i and from R_{j-1} to R_j. The two shells have the same masses (M_i and M_j) as before, and the same semiheights (h_i and h_j). The exact ith zone may be thought of as consisting of the ith thick cylinder, plus a superposed remainder mass distribution (of zero total mass) made up of positive and negative regions near the surface. The total amount of positive mass, m_i, in remainder regions decreases with the number of zones as

$$\frac{m_i}{M_i} \sim \frac{1}{N}$$

for large enough N. Now we have

$$W_{ij}^{\text{int}(E)} = W_{ij}^{\text{int}(I)} + W_{ij}^{\text{RZ}} + W_{ji}^{\text{RZ}} + W_{ij}^{\text{RR}} , \tag{2.10}$$

[1] We thank Dr. George Rybicki for showing us how to do this.

where W_{ij}^{RZ} is the interaction energy of the jth zone and ith remainder, and W_{ij}^{RR} is the remainder-remainder interaction. W_{ij}^{RZ} and W_{ij}^{RR} are estimated by treating the ith remainder as a dipole with mass $\pm m_i$ and separation $R_i - R_{i-1}$:

$$W_{ij}^{RZ} \sim \frac{\partial}{\partial R}\left(\frac{M_j m_i}{|a_i - a_j|}\right)(R_i - R_{i-1}) \sim \left(\frac{M_j M_i}{|a_i - a_j|}\right)\left(\frac{R_i - R_{i-1}}{|a_i - a_j|}\right)\left(\frac{m_i}{M_i}\right) \sim W_{ij}^{int} O\left(\frac{1}{N^2}\right) \tag{2.11}$$

and

$$W_{ij}^{RR} \sim \frac{\partial^2}{\partial R^2}\left(\frac{m_i m_j}{|a_i - a_j|}\right)(R_i - R_{i-1})(R_j - R_{j-1}) \sim W_{ij}^{int} O\left(\frac{1}{N^4}\right). \tag{2.12}$$

So the step from $W_{ij}^{int(E)}$ to $W_{ij}^{int(I)}$ is accurate enough. What about the step from $W_{ij}^{int(I)}$ to W_{ij}^{int} (the thin shell case)? We have exactly

$$W_{ij}^{int(I)} = -2\pi\rho^2 \int_0^{2\pi} d\phi \int_{-h_i}^{h_i} dz \int_{-h_j}^{h_j} dz' \int_{R_{i-1}}^{R_i} dr \int_{R_{j-1}}^{R_j} dr' r r' [(z - z')^2 + r^2 + r'^2 + 2rr' \cos\phi]^{-1}. \tag{2.13}$$

Changing variables by $r \equiv a_i + \xi$, $r' = a_j + \xi'$, and expanding the denominator of equation (2.13), one readily obtains

$$W_{ij}^{int(I)} = W_{ij}^{int} + \left(\text{terms of order } \frac{M_i M_j}{|a_i - a_j|}\frac{1}{N^2}\right). \tag{2.14}$$

The terms that go as $(M_i M_j/|a_i - a_j|)(1/N)$ vanish because they contain only odd powers of ξ and ξ' in the integral. So we again have the accuracy desired.

Now for the self-energy, equations (2.11)–(2.12) with $(R_i - R_{i-1})/|a_i - a_j|$ taken as being of order unity, give the result

$$W_i^{self(I)} - W_i^{self(E)} = W_i^{self(E)} O\left(\frac{1}{N}\right), \tag{2.15}$$

where (I) and (E) mean "intermediate" and "exact" as above. Next observe that we can always find radii b_i and c_i for two thin shells both of mass M_i and semiheight h_i, such that $R_{i-1} \le b_i \le c_i \le R_i$, and such that one-half the interaction energy between them, $\frac{1}{2}W_{bc}^{int}$, equals $W_i^{self(I)}$. (This is obvious, since if $b_i = R_{i-1}$, $c_i = R_i$, then $\frac{1}{2}W_{bc}^{int} < W_i^{self(I)}$; while if $b_i = c_i = R_{i-1}$, then the inequality is reversed.)

For the case in which $h_i \gg (R_i - R_{i-1})$ the two thin shells appear to each other as parallel planes and

$$\frac{\partial \frac{1}{2}W_{bc}^{int}}{\partial b} \approx \frac{\frac{1}{2}W_{bc}^{int}}{b};$$

and a similar equation holds for c. If we compute $\frac{1}{2}W_{bc}^{int}$ for *any* b and c that are within the ith zone but not the exact values that make $\frac{1}{2}W_{bc}^{int}$ equal to $W_i^{self(I)}$, we obtain

$$\frac{1}{2}W_{bc}^{int} - W_i^{self(I)} \approx \Delta b \frac{\partial \frac{1}{2}W_{bc}^{int}}{\partial b} + \Delta c \frac{\partial \frac{1}{2}W_{bc}^{int}}{\partial c} \approx W_i^{self(I)} O\left(\frac{1}{N}\right), \tag{2.16}$$

which is accurate enough. In the other case, in which $h_i \ll (R_i - R_{i-1})$ we must be more careful. Here the ith zone looks like a flat disk for which

$$W_i^{self(I)} = \frac{-8M_i^2}{3\pi(R_i^2 - R_{i-1}^2)}\left[R_i K\left(\frac{R_{i-1}}{R_i}\right)(R_i^2 - R_{i-1}^2) - R_i E\left(\frac{R_{i-1}}{R_i}\right)(R_i^2 + R_{i-1}^2) + R_i^3 + R_{i-1}^3\right], \tag{2.17}$$

where E and K are complete elliptic integrals of the first and second kind (notation as in Dwight 1961). Expanding (2.17) in powers of $(R_i - R_{i-1})/R_i$ gives

$$W_i^{self(I)} = \frac{-M_i^2}{\pi R_i}\left\{-\frac{1}{2}\log\left(\frac{R_i - R_{i-1}}{R_i}\right) + \frac{3}{2}\log 2 + \frac{3}{4} + O\left[\frac{R_i - R_{i-1}}{R_i}\log\left(\frac{R_i - R_{i-1}}{R_i}\right)\right]\right\}. \tag{2.18}$$

The two thin shells appear as two interacting rings, and in this limit

$$\frac{1}{2}W_{bc}^{int} = \frac{-M_i^2}{\pi c} K\left(\frac{b}{c}\right). \tag{2.19}$$

Choosing b and c to lie equidistant from the center of the ith zone, we define $\tilde{b}$ between 0 and 1 by

$$b = \tfrac{1}{2}[(R_i + R_{i-1}) - \tilde{b}(R_i - R_{i-1})], \tag{2.20}$$

$$c = \tfrac{1}{2}[(R_i + R_{i-1}) + \tilde{b}(R_i - R_{i-1})]. \tag{2.21}$$

Expanding equation (2.19),

$$\tfrac{1}{2}W_{bc}{}^{\rm int} = \frac{-M_i^2}{\pi R_i}\left\{-\frac{1}{2}\log\left(\frac{R_i - R_{i-1}}{R_i}\right) + (2\log 2 - \tfrac{1}{2}\log 2\tilde{b}) + O\left[\frac{R_i - R_{i-1}}{R_i}\log\left(\frac{R_i - R_{i-1}}{R_i}\right)\right]\right\}. \tag{2.22}$$

Setting equation (2.18) equal to equation (2.22) gives

$$W_i^{\rm self(I)} = \tfrac{1}{2}W_{bc}{}^{\rm int} + O\left(\frac{1}{N}\right)W_i^{\rm self(I)} \tag{2.23}$$

for $\tilde{b} = \exp(-3/2) = 0.2231$. From these two limiting cases we can see that with this value of $\tilde{b}$, equation (2.23) is now valid in all cases. The prescription for a zone's self-energy is thus: compute one-half the interaction energy of two cylindrical shells of mass M_i, located at fractional distances 0.3884 and 0.6116 into the zone. Since the total self-energies of the zones are of order $1/N$ of the total interaction energies, our computation of W has errors only of order $1/N^2$.

c) *Computation of the Functions* $G(\alpha, \beta)$, $g(\alpha, \beta)$, *and* $\mathcal{G}(\alpha, \beta)$

If we define a function

$$I(\alpha, \beta) \equiv \int_0^\infty dk J_0(k\alpha)J_0(k)\exp(-\beta k), \tag{2.24}$$

then definitions (2.4) and (2.9) yield immediately

$$\frac{\partial g(\alpha, \beta)}{\partial \beta} = I(\alpha, \beta),$$

$$\frac{\partial G(\alpha, \beta)}{\partial \beta} = g(\alpha, \beta),$$

$$\frac{\partial^2 \mathcal{G}(\alpha, \beta)}{\partial \beta^2} = \frac{\partial}{\partial \alpha} I(\alpha, \beta). \tag{2.25}$$

It can be shown, using equation (551.10) from Gröbner and Hofreiter (1949) and equation (8.13.3) from Abramowitz and Stegun (1964), that $I(\alpha, \beta)$ is related to the complete elliptic integral of the first kind $K(\alpha)$, by

$$I(\alpha, \beta) = 2\pi^{-1}[(\alpha + 1)^2 + \beta^2]^{-1/2}K\{2\alpha^{1/2}[(\alpha + 1)^2 + \beta^2]^{-1/2}\}. \tag{2.26}$$

Since there are fast, concise approximations for $K(\alpha)$ and its derivative available (Hastings 1955 or Abramowitz and Stegun 1964, eq. [17.3.34]), we may view I and $\partial I/\partial \alpha$ as known functions. Then the equations (2.25) may be viewed for fixed values of α, as a coupled set of ordinary differential equations to be integrated numerically from $\beta = 0$ to $\beta = \infty$ and tabulated along the way. The initial conditions

$$g(\alpha, 0) = G(\alpha, 0) = \mathcal{G}(\alpha, 0) = \frac{\partial \mathcal{G}(\alpha, 0)}{\partial \beta} = 0 \tag{2.27a}$$

can be verified from the definitions of g, $\mathcal{G}$, and G.

Our particular tabulation of the functions was for arguments $\beta = 0.05\ (0.05)\ 1.0$ and $\beta^{-1} = 0.05\ (0.05)\ 1.0$, and for $\alpha = 0.05\ (0.05)\ 1.0$. From these we constructed new tables for $\bar{g}$, $\bar{G}$, and $\bar{\mathcal{G}}$, where

$$\begin{aligned}
\bar{g}(\alpha, \beta) &\equiv \beta^2[g(\alpha, \beta) - \ln(2\beta)] && (\beta \geq 1)\\
&\equiv \beta^{-1}g(\alpha, \beta) && (\beta < 1),\\
\bar{G}(\alpha, \beta) &\equiv G(\alpha, \beta) - \beta[\ln(2\beta) - 1] && (\beta \geq 1)\\
&\equiv \beta^{-2}G(\alpha, \beta) && (\beta < 1),\\
\bar{\mathcal{G}}(\alpha, \beta) &\equiv \alpha^{-1}\mathcal{G}(\alpha, \beta) && (\beta \geq 1)\\
&\equiv \alpha^{-1}\beta^{-1}\mathcal{G}(\alpha, \beta) && (\beta < 1).
\end{aligned} \tag{2.27b}$$

The function $\bar{g}$ is g with its leading asymptotic terms removed; similarly for $\bar{G}$ and $\bar{\mathcal{G}}$. The barred functions vary very slowly and are always of order unity. Interpolation on them is quite accurate.

Near the boundaries of the tables $\alpha = 0$, $\beta = 0$, and $\beta \to \infty$, the functions cannot be computed accurately enough by the methods already described, so we use the following asymptotic formulae:

$$g(\alpha, \beta \to 0) \approx \frac{2}{\pi}\beta K(\alpha)\,,$$

$$G(\alpha, \beta \to 0) \approx \frac{\beta^2}{\pi} K(\alpha)\,,$$

$$\mathcal{G}(\alpha, \beta \to 0) \approx \frac{\beta^2}{\pi}\frac{\partial}{\partial\alpha} K(\alpha)\,, \tag{2.28}$$

$$g(\alpha \to 0, \beta) \approx \ln\left[\beta + (1 + \beta^2)^{1/2}\right],$$

$$G(\alpha \to 0, \beta) \approx 1 + \beta \ln\left[\beta + (1 + \beta^2)^{1/2}\right] - (1 + \beta^2)^{1/2},$$

$$\mathcal{G}(\alpha \to 0, \beta) \approx \tfrac{1}{2}\alpha[1 - (1 + \beta^2)^{-1/2}], \tag{2.29}$$

$$g(\alpha, \beta \to \infty) \approx \ln(2\beta) + (\alpha^2 + 1)/(4\beta^2),$$

$$G(\alpha, \beta \to \infty) \approx \beta[\ln(2\beta) - 1] + \frac{2}{\pi}(1 - \alpha^2)\left[K(\alpha) + 2\alpha\frac{\partial}{\partial\alpha} K(\alpha)\right],$$

$$\mathcal{G}(\alpha, \beta \to \infty) \approx \frac{2}{\pi}(1 - \alpha^2)\frac{\partial}{\partial\alpha} K(\alpha)\,. \tag{2.30}$$

Neither $\bar{g}(1, 0)$ nor $\bar{G}(1, 0)$ is well defined, but both $g(1, 0)$ and $G(1, 0)$ are, so this presents no problems. $\mathcal{G}(\alpha, \beta)$ is discontinuous at $\alpha = 1$; we always have $\alpha \leq 1$, so we compute the initial value $\mathcal{G}(\alpha = 1^-, \beta \to 0)$ by the asymptotic formula

$$\mathcal{G}(\alpha = 1^-, \beta \to 0) = -\tfrac{1}{2}G(1, \beta) + \frac{\beta^2}{4\pi} - \frac{1}{192\pi}\beta^4 \ln\beta + \frac{\beta^4}{\pi}\left(\frac{\ln 2}{64} - \frac{11}{2304}\right) + O(\beta^6 \ln\beta)\,. \tag{2.31}$$

Thus the integration of equations (2.25) for $\alpha = 1^-$ will typically start at $\beta = 0.05$ (rather than at $\beta = 0$ as for other values of α).

III. STRUCTURE EQUATIONS AND MINIMIZATION METHOD

The plan is to compute a total energy (sum of gravitational and rotational energies),

$$E = W + T\,, \tag{3.1}$$

then to explore its functional behavior and to find equilibrium configurations by extremizing E. The discrete procedure for calculating W was given in equation (2.7) and preceding. The discrete approximation to T is

$$T = \sum_{i=1}^{N} \frac{j_i^2 M_i}{R_{i-1}^2 + R_i^2}\,. \tag{3.2}$$

Here M_i is the mass of the ith zone, and j_i is its angular momentum per unit mass; both of these quantities are conserved and specified *a priori*. By a calculation similar to those of § II*b*, one can show that the fractional error in equation (3.2) due to the discretizing is of order $1/N^2$, where N is the number of zones.

Now it is not immediately obvious that extremizing equation (3.1) with respect to only the R_i's (locations of the zones), holding the j_i's and M_i's fixed, will give equilibrium configurations *and no others*. Certainly true equilibria should be extrema, but one might suspect that there could be "false" extrema, ones which have stationary E for changes in the R_i's, but which might not be extrema of the more general perturbations which do not restrict the rotation to be uniform on vertical cylinders. This is a familiar difficulty in variational problems: we know that an *equilibrium* incompressible configuration must rotate uniformly on cylinders (the famous "Poincaré-Wavre" theorem, cf. Tassoul 1977, § 4.3); but it is not *a priori* safe to impose this constraint before taking the variation: a path which violates the constraint might lead downhill from a "false" extremum to a "true" one (which would, of course, rotate on cylinders).

Luckily, we can show directly that the constraint *can* be imposed before variation in this particular problem. The equation of hydrostatic equilibrium for a rotating star is

$$\frac{1}{\rho}\nabla P = -\nabla(V + \Phi), \tag{3.3}$$

where V is the gravitational potential and Φ is the centrifugal potential defined by

$$\Phi = \int^R dR \frac{j^2}{R^3} \tag{3.4}$$

(cf. Ostriker and Mark 1968, eq. [1], or Tassoul 1977). For an incompressible fluid, equation (3.3) integrates to

$$\frac{P}{\rho} + V + \Phi = \text{constant}. \tag{3.5}$$

This equation has a solution whenever $V + \Phi$ is constant on the surface ($P = 0$) of the body, since then the equation prescribes a self-consistent interior pressure (the incompressible fluid being indifferent to its state of pressure). So we want to see whether the variation of equation (3.1) yields

$$(V + \Phi)_{\text{surface}} = \text{constant}. \tag{3.6}$$

Let $\xi(x)$ be a Lagrangian displacement of fluid elements which is restricted to conserve specific angular momentum and preserve the properties $\partial j(R, z)/\partial z = 0$ (rotation along cylinders) and ρ = constant or zero. Then from

$$T = \int \frac{1}{2}\frac{j^2}{R^2}\, dm \tag{3.7}$$

we have

$$\delta T = -\int \frac{j^2}{R^3}\, \delta R dm = -\int \nabla\Phi \cdot \xi \rho d^3x, \tag{3.8}$$

where Φ is defined in equation (3.4); integrating by parts gives

$$\delta T = -\int \Phi \delta\rho d^3x. \tag{3.9}$$

The equation of continuity,

$$\delta\rho = -\nabla\cdot(\rho\xi), \tag{3.10}$$

has here been used. Notice that $\delta\rho$ is nonzero only at the surface of the body, where it has the values $\pm\rho$ depending only on how the shape has changed. As for W, we have the standard result

$$\delta W = -\int V \delta\rho d^3x \tag{3.11}$$

(cf. Roberts 1963, eq. [29]). So, from equations (3.11) and (3.9) extremization gives

$$0 = \delta E = \int -(V + \Phi)\delta\rho d^3x. \tag{3.12}$$

Not only does $\delta\rho$ lie on the surface, but it has arbitrary changes of sign there, subject only to

$$\int \delta\rho d^3x = 0. \tag{3.13}$$

This is because even the restricted displacements ξ are enough to make arbitrary volume-conserving changes in shape. Therefore, equation (3.12) implies equation (3.6), and we are done with the proof.

A configuration, which may or may not be in equilibrium, is now specified by three sets of numbers. The set $\{M_i\}$ defines a zoning; the set $\{j_i\}$ specifies the angular momentum distribution of the body; and the set $\{R_i\}$ defines the shape of the body. The numerical extremization problem, starting with some initial $E\{R_i\}$, is to adjust the N R_i's until $E\{R_i\}$ is a local minimum. Although some numerical methods for finding minima require only the ability to compute $E\{R_i\}$, methods which can make use of the generalized forces (gradients),

$$F_j\{R_i\} \equiv -\partial E\{R_i\}/\partial R_j, \tag{3.14}$$

are much more powerful.

A variety of function minimization algorithms are reviewed by Acton (1970). One basic technique is to proceed "downhill" in steps, choosing as a direction in N-space the local gradient $\boldsymbol{F}$. This is essentially one form of the "quasi-dynamic method" (QDM) used by Rakavy, Shaviv, and Zinamon (1967) and elaborated on by Kovetz, Shaviv, and Zisman (1976, and references therein). The QDM method has been implemented successfully for models of realistic stars with two-dimensional zoning. Nevertheless, *we do not recommend downhill minimization methods when alternatives are feasible.* Downhill methods have a debilitating disease: they tend to proceed down narrow valleys by taking many sideways "tacks." For a quadratic form in N-space (the simplest function with a minimum), downhill minimization does *not* converge after order N directions; rather, it requires more by a factor in which ratios of the principal axes enter. This factor is typically very large in realistic physical systems, because there typically exist some "small" trial displacements with very large restoring forces (such as smashing a single zone to oblivion).

Fletcher and Powell (1963) have given a very elegant minimization algorithm which avoids these problems. (N.B. The summary of this method in Acton 1970 contains a typographical error.) After one step in a downhill direction, successive gradient directions are modified by a linear transformation which is built up iteratively. The power of the method is that it is *exact* for quadratic forms after N directions (because on the Nth step the linear transformation has become the inverse 2nd partial derivative matrix!). The cost of the method is (i) storage of order N^2 for the linear transformation matrix, and (ii) of order N^2 operations per direction to multiply and update this matrix. For our one-dimensional zoning, $N \sim 30$, these are insignificant costs compared to the advantages realized. Even though $E\{R_i\}$ is not a quadratic form, we usually converge after less than $2N$ directions. Whether the Fletcher-Powell or similar algorithms should be applied to alter the QDM method is an open (and interesting) question. There, with two-dimensional zoning, we may have $N \sim (30)^2$, so that the storage requirement N^2 is becoming large. One would want to compare the Fletcher-Powell algorithm both to the explicit QDM downhill method, and to the implicit scheme of Kovetz, Shaviv, and Zisman (1976) which requires the inversion of a tri-diagonal block matrix.

Our criterion for convergence is

$$\left|\frac{F_i R_i}{E}\right| < \epsilon \quad \text{for all } i = 1, \ldots, N. \tag{3.15}$$

Typically we take $\epsilon = 10^{-6}$.

IV. THE MACLAURIN ANGULAR MOMENTUM DISTRIBUTION

a) *Maclaurin Spheroids*

The Maclaurin spheroids are uniformly rotating, equilibrium bodies parametrized by their eccentricity e. For a given total mass M and density ρ, their total angular momentum L increases monotonically with e. We will want to parametrize the sequence by L (not e) or by its nondimensional equivalent

$$L_* \equiv \left(\frac{4\pi}{3}\right)^{1/6} LG^{-1/2}M^{-5/3}\rho^{1/6} \tag{4.1}$$

(G is the gravitational constant), since e is not so meaningful for shapes other than spheroidal. The relation between e and L_* is (Chandrasekhar 1969, hereafter cited as EFE)

$$L_*{}^2 = \tfrac{3}{25}(1 - e^2)^{-2/3}\left[\frac{2(1 - e^2)^{1/2}}{e^3}(3 - 2e^2)\sin^{-1} e - \frac{6}{e^2}(1 - e^2)\right]. \tag{4.2}$$

The angular momentum distribution of a uniformly rotating spheroid obviously has the same functional form as that of a uniformly rotating sphere. In detail this turns out to be

$$l_*(m) = L^*\left[1 - \frac{5}{2}\left(1 - \frac{m}{M}\right) + \frac{3}{2}\left(1 - \frac{m}{M}\right)^{5/3}\right]. \tag{4.3}$$

Here m ($0 \leq m \leq M$) is the total mass interior to a cylinder of some radius, and $l_*(m)$ is the total nondimensional angular momentum within this same cylinder.

We have applied the minimization method of § III to this angular momentum distribution. Typically we use 20 zones and choose the M_i's so that the R_i's are equally spaced if the fluid is a spheroid, and then use these R_i's as the initial guesses. The j_i's are computed from equation (4.3). For $e < 0.99892$, corresponding to $L_* < 0.965175$, the Maclaurin sequence is known to be dynamically stable to small *axisymmetric* perturbations (EFE, § 33). Therefore, we expect only very small adjustments in the R_i's before a minimum is reached. This is in fact found. Our computed total energy for, say, $e = 0.7$, is within 0.07% of the analytically calculable Maclaurin spheroid energy (see EFE, § 32), and our calculated rotation curve is uniformly rotating to an accuracy of 0.4% (with errors about equally positive and negative). These results are not just due to the "judicious" initial guesses; the dimensionless forces (eq. [3.15]) were reduced by three orders of magnitude by the minimization routine, and we also

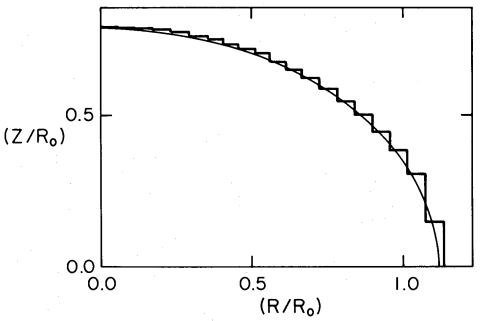

FIG. 1.—Shape of 20 zone model found by energy minimization. The Maclaurin spheroid with the same angular momentum (eccentricity $e = 0.7$) is also shown. Energies of the two shapes agree within 0.07%. Lengths are measured in units of R_0, the radius of the sphere of equal volume.

converge to precisely the same values from initial guesses that are greatly different from the Maclaurin spheroid R_i's. We have also checked that the error in energy decreases with number of zones as $1/N^2$, confirming the estimates in § III*b*. Figure 1 shows the shape of our model superposed on an actual ellipse of eccentricity 0.7.

b) *New "Maclaurin Toroids"*

If $L_* > 0.965175 \equiv L^+$, the Maclaurin spheroids are dynamically unstable to axisymmetric perturbations. Therefore, the extremum of our variational method is a saddle, and the minimizing algorithm will not converge to it. Instead it converges to a new shape, the one which the spheroid's instability is "trying" to take it to. Before doing the experiment, we expected that this new shape would be a centrally condensed disk, like that of Mestel (1963; see § IV*d* below). But instead, the new shape turns out to be that of a differentially rotating toroid. At $L_* = L^+$, the total energy of the toroid is $\sim 3\%$ less than the corresponding spheroid. Figure 2*a* shows the cross section of this toroid superposed on that of the marginally stable spheroid, and Figure 2*b* shows its angular momentum as a function of radius. The toroid's polar minor radius is about half its equatorial minor radius. Its inner edge is not rotating at all, but rather is held outward by the gravitational attraction of the toroid. (The matter here was formerly on the axis of the spheroid and has no angular momentum.) The outer edge is rotating slightly faster than the angular velocity of the corresponding spheroid.

Now varying L_*, we find that the toroid at $L_* = L^+$ is just one member of a whole sequence of "Maclaurin toroids." As we increase L_*, the toroids remain stable against axisymmetric disturbances (insofar as we can determine). They do not break up into two or more rings, or into a disk. The radius of the rings is always less than,

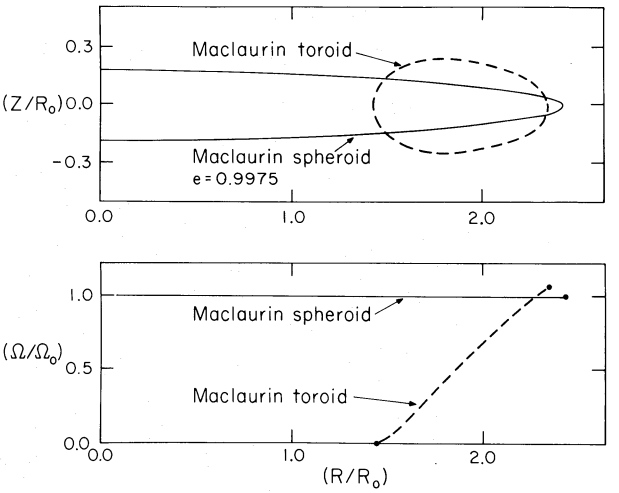

FIG. 2.—(*a*) (*top*) Cross section of marginally stable Maclaurin spheroid, eccentricity $e = 0.9975$ (*solid line*) and stable Maclaurin toroid (*dashed line*). The energy of the toroid is $\approx 3\%$ lower than that of the spheroid. Lengths are measured in units of R_0 as in Fig. 1. (*b*) (*bottom*) Angular velocity, Ω, of the differentially rotating Maclaurin toroid of Fig. 2*a* (*dashed line*) as a function of distance from the axis of rotation. Angular velocity is measured in units of Ω_0, the angular velocity of the rigidly rotating spheroid (*solid line*). The toroid's inner edge is not rotating and is supported only by gravitational attraction to the mass of the toroid.

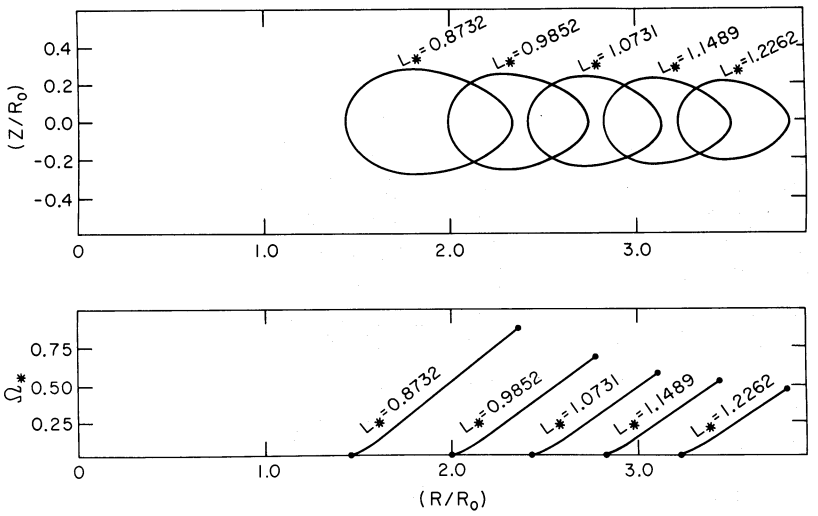

FIG. 3.—(*a*) (*top*) Cross sections of some Maclaurin toroids. The dimensionless angular momentum, $L_* = (4\pi/3)^{1/6} L G^{-1/2} \times M^{-5/3} \rho^{1/6}$ varies, while M and ρ are kept constant. The distribution of angular momentum per unit mass is the same as that of a rigidly rotating spheroid. Lengths are in the same units as Fig. 1. (*b*) (*bottom*) Rotation curves of the toroids shown in Fig. 3*a*. Shown is the angular velocity Ω_* [angular velocity in units of $(G\rho)^{1/2}$] as a function of distance from the axis of rotation.

but on the same order as, the radius of the corresponding (unstable) spheroid. The rings never become very flattened; the ratio of their minor radii stays at about 2. Figure 3*a* shows the cross section of several Maclaurin toroids, and Figure 3*b* plots the corresponding rotation curves. The angular velocity of the outer edge of the toroid is always of the same order as the corresponding Maclaurin spheroid. We have followed the sequence up to $L_* \approx 3.5$, corresponding to $e \approx 1 - 10^{-10}$ or a ratio of spheroid axes of $\sim 10^{-5}$.

As L_* decreases from L^+, the toroidal sequence also continues. At $L_* = 0.792 \pm 0.002 \equiv L_0$ ($e = 0.9949 \pm 0.0001$) the toroid total energy crosses that of the spheroid. One might have thought that stability passes to the

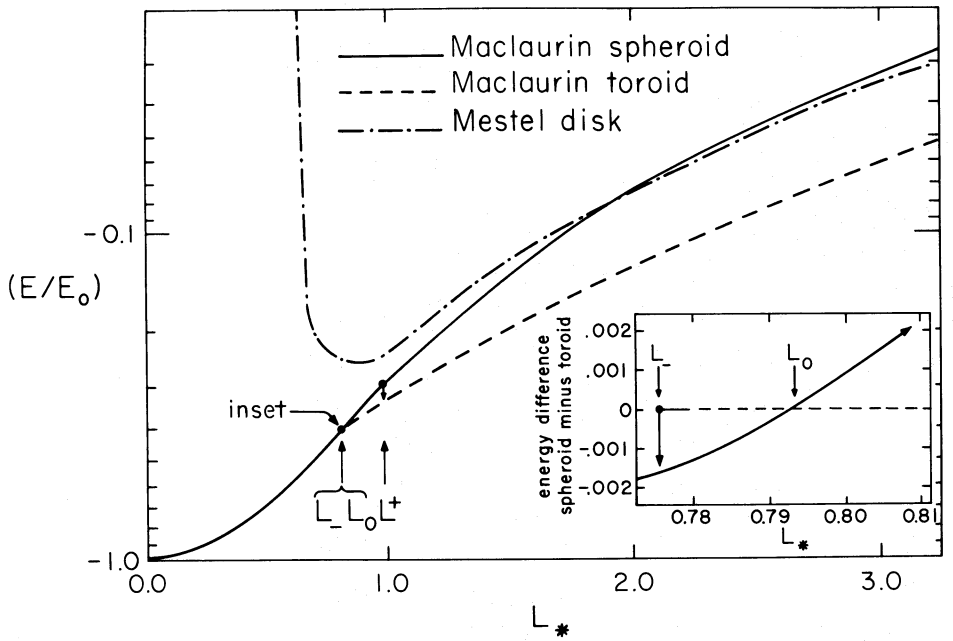

FIG. 4.—Total energy of the Mestel disk, Maclaurin spheroid, and Maclaurin toroid as a function of angular momentum. Energy is measured in units of $|E_0|$, the energy of a nonrotating sphere of equal mass and volume. L_* is the dimensionless angular momentum as in Fig. 3*a*. The inset is the difference in energy between the spheroid and the toroid. When $L_* = L_0 = 0.792$ the energies are equal. For $L_0 \leq L_* \leq L^+ = 0.965$ the spheroid is stable to small perturbations but the toroid has lower energy. For $L_0 \geq L_* \geq L_- = 0.775$ the toroid is stable, but the spheroid has lower energy. Solid circles mark onsets of instability. The Mestel disk is never stable. Disk, spheroid, and toroid have identical distributions or angular momentum per mass element.

spheroid at this point, but in fact this point has no special dynamical significance for either toroid or spheroid. When L_* has decreased further $\sim 0.775 \equiv L_-$ ($e \sim 0.994$), the toroids become unstable and we drop down to the spheroid sequence, whose energy is now 0.4% lower. Figure 4 summarizes these results. One sees that, for L_* between L_0 and L^+, the Maclaurin spheroids are actually *metastable* to axisymmetric disturbances: they are stable against small perturbations, but a sufficiently large perturbation will push them into the lower-energy toroid "valley." We have verified this by converging our program from a variety of initial guesses. No initial guess, however bizarre, converted to any third shape; we therefore think that the toroids are the *global* minimum. (Incidentally, we were not able to converge to spheroids all the way up to [analytically known] L^+; at values slightly less, the metastable spheroid "valley" is so small that we are not able to find initial guesses in it—we instead drop down to the toroid sequence. Discretization errors must also come into play.)

For L_* between L_- and L_0, the spheroids seem to be global minimum, and the toroids are metastable. Below L_- the toroids are unstable, and we have no way of knowing how far the sequence continues.

c) *Comparison with Dyson Toroids, and* $|T/W|$

Toroidal fluid bodies with a uniform (rigid) rotation law have been investigated previously, notably by Dyson (1892, 1893) and recently by Wong (1974) who gives further references. These bodies do not have the same distribution of angular momentum with mass as the Maclaurin spheroids; only processes which transport angular momentum could induce a transition from a Maclaurin spheroid to a Dyson-Wong toroid. Bardeen (1971) has noted that the total energy of the Dyson rings crosses that of the Maclaurin sequence very nearly at the angular momentum value where *secular* axisymmetric instability sets in, while the energy of our toroidal sequence crosses nearer the dynamic instability point L^+. A fair amount is known about the *nonaxisymmetric* stability (or lack thereof) of the uniformly rotating toroids. Let us see what further comparisons can be made between the Dyson-Wong and Maclaurin toroidal sequences:

One proposed indicator of body's dynamic stability (Ostriker and Bodenheimer 1968) is the ratio of its rotational energy to its potential energy, $|T/W|$. Figure 5 shows this quantity as a function of L_* for the Maclaurin spheroids and toroids, and Dyson-Wong toroids. The spheroid values are given analytically by

$$|T/W| = \frac{1}{2}\frac{[(3 - 2e^2)\sin^{-1} e - 3e(1 - e^2)^{1/2}]}{e^2 \sin^{-1} e} . \tag{4.4}$$

The toroidal values are from our numerical work and from Wong (1974). Notice that the Maclaurin ring has a lower ("more stable") value than the spheroid, and *decreases* with increasing L_* at least up to $L_* = 3.5$. It would be interesting to know whether this decrease continues indefinitely. (We encounter numerical difficulties at $L_* = 3.5$ and have not proceeded further.) For the Dyson-Wong sequence $|T/W|$ decreases until a minimum value is reached at $L_* \approx 0.69$, and then increases again.

Although it is not rigorously known in the inviscid case, the Dyson-Wong toroids are probably all unstable against "beaded" displacements which lead to their fragmentation into separately orbiting lumps. How can we estimate whether the Maclaurin toroids are more or less stable to these modes? One rough way (Ostriker, unpublished; Wiita and Press 1976) is to break up the toroids by fiat into $n \geq 2$ equal spheres in a circular orbit, conserving total mass, angular momentum, *and circulation in the midplane.* One then sees whether the total energy of the system has increased (indication of its stability) or decreased (indication of instability). We have done this calculation for several values of L_*. For $L_* = 0.979$, the Dyson toroid is indicated unstable for all n. The Maclaurin

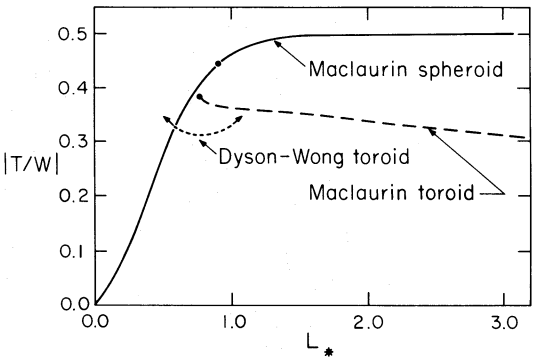

FIG. 5.—Stability indicator $|T/W|$ as a function of angular momenta for the Maclaurin spheroid, Maclaurin toroid, and Dyson-Wong (uniformly rotating) toroid. T and W are the rotational and potential energies, respectively. Solid circles indicate where the sequences become unstable. For values of L_* greater than 1.2 the Maclaurin toroids have the lowest $|T/W|$, suggesting that they may have the greatest stability. Note that the Dyson-Wong toroids have a different distribution of angular momentum from the two Maclaurin sequences.

toroid is indicated *stable* for $n = 2, 3, 4, 5$, and unstable for larger n. Of course, at some large n the method is not reliable anyway, since the supposed spheres start overlapping. For a larger $L_* = 2.69$, the Dyson toroid still seems unstable for all n, while the Maclaurin seems stable for $n = 2, 3, \ldots, 47$. The explanation is that the large circulation implied by the differential rotation of the Maclaurin toroid imposes a strong constraint on the rotational velocities and orbital radius of the spheres. This fact, coupled with decreasing $|T/W|$ raises the interesting possibility that the Maclaurin toroids might actually be stable to *all* infinitesimal perturbations, at least for some high values of L_*!

d) Mestel Disks with the Maclaurin Angular Momentum Distribution

Mestel (1973) found yet another shape which is an equilibrium configuration of the angular momentum law (4.3), at least in the limit of very flat bodies (very large L_*). In the language of incompressible fluids, Mestel's disk has semiheight.

$$h(R) = \frac{3}{8\pi}\frac{M}{R_0\rho}\frac{1}{R}\left(1 - \frac{R}{R_0}\right)^{1/2}, \tag{4.5}$$

where R_0 is an outer radius, related to L (or L_*) by

$$R_0 = \tfrac{25}{6}L^2G^{-1}M^{-3}. \tag{4.6}$$

This configuration is a centrally condensed disk with a constant-velocity rotation curve:

$$V(R) = R\Omega(R) = \left(\frac{3}{2}G\frac{M}{R_0}\right)^{1/2}. \tag{4.7}$$

which makes it interesting as a galactic model. The disk is a precise equilibrium only in the limit $R_0 \to \infty$. Nevertheless, we originally expected that for finite R_0 we might use this disk as a starting guess and then converge to a precise equilibrium only slightly different. In fact, there seems to be no nearby energy minimum for *any* R_0 (or L_*). The existence of nearby extrema is confirmed by the fact that the starting values of the nondimensional forced F_iR_i/E are very small; but the minimization algorithm always traverses a large distance away from the extremum to settle on a Maclaurin spheroid or toroid which is a true minimum. In Figure 4, the energies of the initial near-extrema are plotted. One sees that a toroid or spheroid always has a lower energy. From these results we conclude that these fluid Mestel disks are always unstable to axisymmetric perturbations, and are neither local nor global energy minima.

This conclusion can be compared to the predictions of the local (high-wavenumber) disk stability tests due to Toomre (1964) and Goldreich and Lynden-Bell (1965). For fluid disks, both criteria give the inequality $\pi G\rho/4\Omega^2 >$ constant, for instability. For the Goldreich and Lynden-Bell test the constant is 1.75, and our Mestel disks are stable by this test over their whole surface whenever $L_* < 0.763$. For the Toomre test, the constant is smaller by a factor which can be as large as ~ 8 (depending on the assumptions under which one translates from stellar-dynamic to perfect-fluid formalism). However, the critical value of L_* varies only as the one-sixth power of this constant. As one expects, the local test indicates *instability* reliably, but global instabilities do occur even when the local test is not violated.

V. OTHER DISTRIBUTIONS OF ANGULAR MOMENTUM

Mestel (1963) discovered another thin-disk equilibrium configuration, with

$$h(R) = \frac{M}{4\pi R_0 R} \quad (R < R_0)$$
$$= 0 \qquad (R > R_0), \tag{5.1}$$

$$V(R) = R\Omega(R) = (GM/R_0)^{1/2}, \tag{5.2}$$

and a corresponding angular momentum distribution

$$l_*(m) = L_*(m/M)^2. \tag{5.3}$$

The functional shape of this $l_*(m)$ is generally similar to the Maclaurin one (eq. [4.3]). Its difference in detail furnishes the opportunity to see whether the conclusions of § IV are sensitive to the angular momentum distributions chosen. In brief, the answer is that they are not. We are never able to converge to the Mestel disk (5.1). Instead we converge to an "almost"-spheroid which rotates "almost" rigidly, or else to a toroid in differential rotation. The value of L_* where the toroid and spheroid sequences cross in energy is almost identical to the Maclaurin L_0 value found above, and other critical values are also similar. Again we have found that at least some members of this unstable sequence do not violate the *local* stability criteria.

Another way of constructing a non-Maclaurin angular momentum distribution is to choose any desired height profile for the disk (as a function of radius), then compute the radial generalized forces due to gravity by the methods of § II, and finally compute the angular momenta J_i which are necessary to make this shape an equilibrium. If any J_i come out imaginary, then the shape is impossible. Even when the shape is possible, it might not be radially stable; so the minimization algorithm is invoked, and the shape may converge to a totally different one. When we apply this procedure to the Mestel profiles of equations (4.5) and (5.1), the results are indistinguishable from those already described. For another test we invented a two-parameter family of profiles:

$$h(r) = \frac{M}{4\pi\rho a_0[(a_0^2 + R_0^2)^{1/2} - a_0]}\left[1 + \left(\frac{R}{a_0}\right)^2\right]^{-1/2} \quad (R < R_0)$$
$$= 0 \quad (R > R_0)\,. \tag{5.4}$$

These are "bulge-disk" configurations, with central spheroidal bulges whose scale is set by the parameter a_0, and tapered disks extending out to a radius R_0. We chose the shape to be reminiscent of an S0 galaxy seen edge-on. Not surprisingly, the computed rotation curves for these profiles are also reminiscent of galactic rotation curves, almost flat out to the edge of the disk.

All of the profiles (5.4) are radially *unstable*. They go, as does everything else we have looked at, either to approximate spheroids with approximately uniform rotation, or else to differentially rotating toroids. These profiles are, incidentally, unstable even by the local tests; but the global toroid mode dominates their energy-minimizing "evolution."

VI. DISCUSSION

Our search for energy minima, which are likely to correspond to preferred "channels" of a dynamical evolution, turned up precisely two, the spheroid-like and toroid-like shapes. The transition between these seems governed by total angular momentum in nondimensional units, L_*. The omnipresence of toroids for large L_*, while unexpected, may help explain in a unified way results such as those of Black and Bodenheimer (1976), who find that collapsing, rotating protostars go through a ring phase, and those of Larson (1972) who finds some protogalaxies collapsing to toroids under physical conditions very different from the stellar-collapse case. Axisymmetric stellar dynamical models by Prendergast and Tomer (1970) and by Gott (1973) also show toroidal features.

Our inability to find stable figures with galaxy-like profiles or rotation curves is more puzzling; Mestel disks in two varieties, and the two-parameter family (5.4), are all unstable. One possible resolution of the puzzle is if the instability is an artifact of our fluid's incompressibility. We do not think this is so: the incompressible disk is so thin that density changes in the direction parallel to the rotation axis affect the dynamics hardly at all. A compressible disk would certainly lack the central spike of the incompressible Mestel figures, but the total mass in the spike is very small. We have computed a few models of a disk of uniform thickness $\sim 1/100$ of the radius R_0, but with variable density so that

$$m(R) \propto \frac{1}{R}\left(1 - \frac{R}{R_0}\right)^{1/2}. \tag{6.1}$$

The rotation curves were almost identical to the models of equation (4.5). These compressible disks were also all unstable, even when they satisfied the local stability tests by a safe margin (they did have high values of $|T/W|$, however, ~ 3). Our referee has suggested some further models whose stability or instability might indicate whether compressibility is an important feature: (i) a Mestel disk with $h \propto r$ and $\rho \propto r^{-2}$, since the local tests are satisfied *by a constant factor* over the surface of this disk; (ii) compressible and incompressible versions of the exponential disks of Freeman (1970) and the double exponential disks of Hohl (1971).

A second resolution is if the stellar-dynamic nature of real galaxies is crucial in stabilizing the disk. This cannot be ruled out; however, Toomre's (stellar-dynamic) local criterion for stability is typically *more* stringent for the disks we have looked at than its perfect fluid (Goldreich-Lynden-Bell) counterpart, so it is hard to find an effect in the right direction even!

A third possibility, which we favor, is the massive halo hypothesis of Ostriker and Peebles (1973) and others. The massive halo has previously been invoked as a defense against nonaxisymmetric, bar instabilities. We suggest that the halo *may* also be necessary to stabilize realistic models against purely radial readjustments, into spheroids (i.e., elliptical galaxies) or toroids (ring galaxies?? cf. Freeman and de Vaucouleurs 1974; Theys and Spiegel 1976; however, Toomre has advanced a very compelling alternative theory, cf. Lynds and Toomre 1976).

Finally some remarks concerning the computational techniques of this paper: We think that minimization algorithms, *when more sophisticated than just stepping down a gradient*, may be a fruitful approach for a variety of problems where there is an underlying variational principle. The QDM method (see § III) deserves further attention. We also think that more can be done with the finite cylinder method of calculating gravitational potentials, described in § II. At the very least it is an efficient way of computing finite-thickness corrections to disk models of galactic rotation: even though the density in the z-direction will not be constant, the finite thickness enters in first

order only as an effective density and scale height (details will be given elsewhere). Superposing more than one cylinder at a given radius, one can model a general rotating star. This technique may have advantages over other schemes of two-dimensional zoning, because the number of vertical zones necessary for an accurate potential calculation may be very small (i.e., four or five per radial zone) if their heights are chosen correctly.

Discussions with A. G. W. Cameron, S. Chandrasekhar, and J. P. Ostriker have benefited us in this work. We thank the referee for a number of suggestions.

REFERENCES

Abramowitz, M., and Stegun, I. A. 1964, *Handbook of Mathematical Functions* (Washington: National Bureau of Standards).
Acton, F. S. 1970, *Numerical Methods That Work* (New York: Harper & Row).
Bardeen, J. M. 1971, *Ap. J.*, **167**, 425.
Black, D. C., and Bodenheimer, P. 1976, *Ap. J.*, **206**, 138.
Cameron, A. G. W., and Pine, M. R. 1973, *Icarus*, **18**, 377.
Chandrasekhar, S. 1969, *Ellipsoidal Figures of Equilibrium* (New Haven: Yale University Press) (EFE).
Dwight, H. B. 1961, *Tables of Integrals and Other Mathematical Data* (New York: Macmillan).
Dyson, F. W. 1892, *Phil. Trans. Roy. Soc. London, A*, **184**, 33.
———. 1893, *Phil. Trans. Roy. Soc. London, A*, **184**, 1041.
Fletcher, R., and Powell, M. J. D. 1963, *Computer J.*, **6**, 163.
Freeman, K. C. 1970, *Ap. J.*, **160**, 811.
Freeman, K. C., and de Vaucouleurs, G. 1974, *Ap. J.*, **194**, 569.
Goldreich, P., and Lynden-Bell, D. 1965, *M.N.R.A.S.*, **130**, 97.
Gott, J. R., III. 1973, *Ap. J.*, **186**, 481.
Gott, J. R., III, and Thuan, T. X. 1976, *Ap. J.*, **204**, 649.
Gröbner, W., and Hofreiter, N. 1949, *Integraltafel* (Vienna: Springer-Verlag).
Hastings, C., Jr. 1955, *Approximations for Digital Computers* (Princeton: Princeton University Press).
Hohl, F. 1971, *Ap. J.*, **168**, 343.
Kovetz, A., Shaviv, G., and Zisman, S. 1976, *Ap. J.*, **206**, 809.
Larson, R. E. 1972, *M.N.R.A.S.*, **156**, 437.
Lynds, R., and Toomre, A. 1976, *Ap. J.*, **209**, 382.
Mestel, L. 1963, *M.N.R.A.S.*, **126**, 553.
Morse, P. M., and Feshbach, H. 1953, *Methods of Theoretical Physics* (New York: McGraw-Hill).
Ostriker, J. P., and Bodenheimer, P. 1968, *Ap. J.*, **151**, 1089.
Ostriker, J. P., and Mark, J. W-K. 1968, *Ap. J.*, **151**, 1075.
Ostriker, J. P., and Peebles, P. J. E. 1973, *Ap. J.*, **186**, 467.
Prendergast, K. H., and Tomer, E. 1970, *A.J.*, **75**, 674.
Rakavy, G., Shaviv, G., and Zinamon, Z. 1967, *Ap. J.*, **150**, 131.
Roberts, P. H. 1963, *Ap. J.*, **137**, 1129.
Tassoul, J. L. 1977, *The Theory of Rotating Stars* (monograph in preparation).
Theys, J. C., and Spiegel, E. A. 1976, *Ap. J.*, **208**, 650.
Toomre, A. 1964, *Ap. J.*, **139**, 1217.
Wiita, P. J., and Press, W. H. 1976, *Ap. J.*, **208**, 525.
Wong, C. Y. 1974, *Ap. J.*, **190**, 675.

PHILIP S. MARCUS and WILLIAM H. PRESS: Center for Astrophysics, 60 Garden Street, Cambridge, MA 02138
SAUL A. TEUKOLSKY: Department of Physics, Cornell University, Ithaca, NY 14853